# Chapter 1
# An Introduction to the Wonder 2D Nanomaterials: Synthetic Approaches and Fundamental Properties


**Amit K. Rana and Amreen A. Hussain**

## 1 Introduction

Nanomaterials have been attracting the scientific world because of their unusual physiochemical characteristics due to their high aspect ratio, strange surface morphology, unique surface chemistry, and quantum-size effect, as compared to their bulk counterparts [1]. Based on their unique properties, they can be applied in a wide range of multifunctional application. In the last few decades, a large number of research works are published in the field of nanomaterials with a progressing span of about 30,000 publications per year. Dimensionality is one of the key factors to manipulate the nanomaterial properties. It is to be noted that the properties of nanomaterials are mostly attributed to their unique nanostructure and composition. Moreover, in terms of dimensions or confinement of electrons, nanomaterials have been categorized as zero (0D-), one (1D-), and two (2D-) nanostructures. For instance, the 0D nanomaterials (such as spherical nanoparticles and quantum dots) confine electrons in all three dimensions in the nanometre range. Similarly, with 1D and 2D structures, the electrons are confined in either one or two dimensions (2D) in the nanometre range [1]. In this chapter, we are interested to discuss different types of 2D nanomaterials along with their synthetic approaches, properties, and material characterizations.

In 2004, Novoselov and co-workers exfoliated a single-atom-thick layer of graphite using a mechanical cleavage method where the carbon atoms are arranged in a 2D hexagonal structure, which led to the discovery of Nobel Prize-winning

A. K. Rana (✉)
Department of Materials Science and Engineering, Ulsan National Institute of Science and Technology (UNIST), Ulsan 44919, South Korea
e-mail: aramitrana4@gmail.com

A. A. Hussain
Facilitation Centre for Industrial Plasma Technologies (FCIPT), Institute for Plasma Research (IPR), Gandhinagar 382428, Gujarat, India
e-mail: amreenhussain8888@gmail.com



Z. Khanam et al. (eds.), *2D Nanomaterials for Energy and Environmental Sustainability*,
Materials Horizons: From Nature to Nanomaterials,
https://doi.org/10.1007/978-981-16-8538-5_1

graphene [2]. With the discovery of graphene, the scientific community has received a lot of attention to exploring the other potential 2D nanostructures. Therefore, after years of hard work, the scientists working in the field of 2D nanomaterials have found novel ways to synthesize 2D nanomaterials such as mechanical cleavage, ion-intercalation, liquid exfoliation, chemical vapour deposition (CVD), plasma-enhanced chemical vapour deposition (PECVD), hydrothermal syntheses [3–6]. For the synthesis of 2D nanomaterials, a large variety of materials are explored: from metals to semiconductors to insulators and even to superconductors which show remarkable properties with better performance than graphene. Based on the electron confinement in single-layered 2D nanomaterials, they show outstanding electronic and transport properties. In addition, the nanomaterials have a high surface area, owing to the exposure of edge sites, and flexibility in atomic level, high thermal endurance which made them suitable candidates for diverse applications such as in nano-electronics, optoelectronics, medical, civil fields and in space applications [5–7].

## *1.1 Type of 2D Nanomaterials*

As already highlighted, graphene is known as a wonder nanomaterial consisting of crystalline carbon film and exhibits various unprecedented properties, such as ultrahigh carrier mobility (~10,000 $cm^2\ V^{-1}\ s^{-1}$), quantum hall effect, high specific surface area (2630 $m^2\ g^{-1}$), optical transparency (~97.7%), and excellent thermal conductivity (3000–5000 $W\text{-}m^{-1}\ K^{-1}$) [2]. Inspired by the unexpected properties of graphene, the quest to explore other ultrathin 2D nanomaterials begins. Efforts are made by the researchers to exploit new 2D nanomaterials that possess similar features to that of graphene, yet capable of versatile properties. Among the family of new 2D materials originates the transition metal dichalcogenides (TMDs; e.g. $MoS_2$, $NbSe_2$, $TaS_2$, $WS_2$, $MoSe_2$, $WSe_2$, etc.), hexagonal boron nitride (h-BN), carbon nitride (CN), transition metal oxides, layered perovskites, metal–organic frameworks, black phosphorus (BP), and MXenes [7–11], as schematically presented in Fig. 1.

***Transition metal dichalcogenides (TMDs)***: TMD monolayers are semiconductor materials with atomically thin layers with a general representation of $MX_2$; where M is a transition metal (Mo, W, Te, etc.), and X is a chalcogen atom (X = S, Se, Te, etc.). In a typical structure of $MX_2$, one layer of M atoms is sandwich between two separate layers of X atoms to form X–M–X structure [10]. With this atomic arrangement, the crystal structure forms a honeycomb, hexagonal lattice. Usually, the M–X bonds (intralayer) between the transition metal and chalcogen atoms are known to be covalent bonds, whereas the individual $MX_2$ layers are bonded together by van der Waals (vdW) (interlayer) forces which are considered as weak bonds. Moreover, the TMDs can form metal coordination such as trigonal prismatic or octahedral. This coordination of metals and also the order of staking between the monolayers describe the phase of TMD materials. Some most common phases are

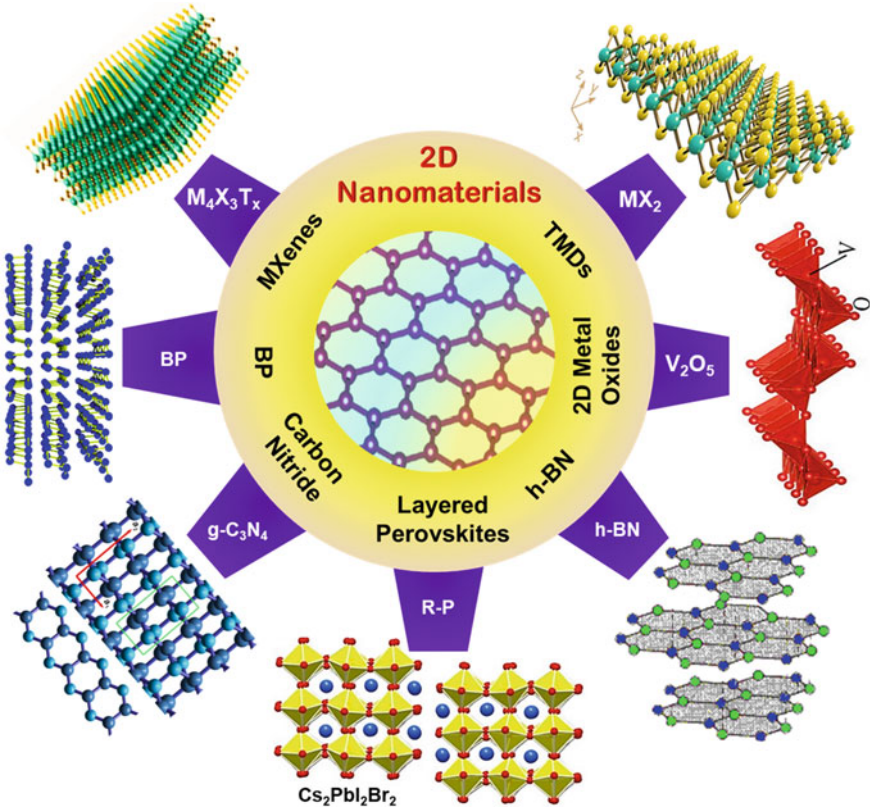


**Fig. 1** Schematic illustration of different kinds of typical ultrathin 2D nanomaterials, such as graphene, h-BN, TMDs, MXenes, TMOs (2D metal oxides), layered perovskite, and BP (phosphorene)

1T, 2H, or 3R, where T, H, and R stand for tetragonal, hexagonal, and rhombohedral, while 1, 2, and 3 denote the number of X–M–X sandwiches per unit cell.

***Hexagonal boron nitride (h-BN)***: h-BN is a layered material that has a similar structure to graphite, which in turn has similar properties like graphite. The crystal arrangement of h-BN consists of alternate boron and nitrogen atoms which is bonded with $sp^2$ hybridization forming an atomic-level thick layer [11, 12]. Usually, the bond length among two consecutive boron and nitrogen atoms is 0.144 nm. h-BN exhibits covalent bonding within the plane. Irrespective of this, its interplane bonding is relatively weak due to vdW forces. In h-BN, the spacing between two successive layers is 0.334 nm which is analogous to graphene (0.333 nm). Thus, h-BN displays advantages for efficient electronic and optical applications.

***Carbon nitride (CN)***: Graphitic carbon nitride (general formula g-$C_3N_4$) is one of the hardest and most stable compounds belonging to the library of 2D nanomaterials.

The fundamental structure of $C_3N_4$ forms a polymeric stacked structure which is more like graphite containing $sp^2$ hybridized carbon and nitrogen atoms [13]. It consists of tris-triazine-based patterns where the carbon to nitrogen ratio is typically ¾ with a small amount of hydrogen. Because of the presence of nitrogen (lone pair) and π-conjugation system with carbon $p_z$-orbital, the $C_3N_4$ shows promising electronic properties. There are mainly two known structures of $C_3N_4$, one is based on heptazine, and the other is poly-triazine imide units based on which the reaction conditions, reactivities, and the associated properties can vary.

***Transition metal oxides***: The transition metal oxides from their bulk state can be transformed into atomically thin nanosheets, thus placing their stand as 2D nanomaterials [14]. It is already known that the bulk metal oxides can show unique combination of both physical and chemical properties with earth abundance. However, the 2D nanosheets of metal oxides provide even more unprecedented features such as larger surface area, improved active sites, and interplanar charge transport. There are various metal oxides found in nature, and to name a few are $MoO_3$, $TiO_2$, ZnO, $Co_3O_4$, $V_2O_5$, etc. Every 2D metal oxides have different crystal structures which will be discussed in detail in the succeeding sections of the chapter.

***Layered perovskites***: The dimensionality of the 3D perovskite structure when reduced to layered 2D form enables very interesting properties for diverse applications. In simple terms, the 2D perovskite resembles the slice cut from the 3D perovskite lattice. Different from the 3D perovskite with $ABX_3$ structure (where a larger cation (A) simply fills the voids between $BX_6$ octahedra), and in 2D perovskite, some larger cations are introduced into the structure with acts as spacers [15]. These spacers help to isolate the inorganic octahedra to form quantum well superlattices. Furthermore, these extra spacing cations induce asymmetric lattice structure, thereby providing an additional degree of freedom. Thus, the structural slicing along a definite crystallographic plane forms a layered material that is coupled by weak vdW interactions. The empirical formula of 2D perovskites is $L_2MX_4$, where L is the large monovalent organic cation/spacer, M the metal cation, and X the anion. Few examples of 2D-layered perovskites are $Cs_2PbI_2Br_2$, $(BA)_2(MA)_2Pb_3I_{10}$, etc.

***Metal–Organic frameworks***: Metal–organic frameworks also form 2D structures which are considered as an attractive alternate crystalline porous material [16, 17]. It basically consists of metal bridging nodes and multi-podal organic ligands that are bonded together. This type of bonding usually forms through basic coordination chemistry. In general, the metal node is coupled to the organic ligand by a coordination bond; however, the layers of the metal–organic framework are linked by weak vdW forces.

***Elemental 2D nanomaterials***: Elemental 2D nanomaterials are attracting great attention with the experimental demonstrations of borophene nanosheets belonging to the group III. Boron forms almost 16 number of allotropes through complex B–B bonds, out of which only three forms are thermodynamically stable (α-rhombohedral, β-rhombohedral, γ-orthorhombic, and γ-tetragonal) [18]. These allotropes consist of the icosahedral $B_{12}$ units as the building blocks. Notable structure among the

borophene is the $B_{36}$, which has a bowl-shaped cluster with a periodic hexagonal holes arrangement forming a triangular lattice. The hexagonal arrangements of atoms can be visualized as graphene-like nanosheets [18, 19].

Another interesting 2D nanomaterials are silicene, germanene, and stanene belonging to the group IV elements [19]. Silicene is derived from silicon which comprises a buckled sheet and can host non-trivial electronic states, spin-polarized edges, and a tunable bandgap that allows for application in quantum information. Similarly, germanene is also a buckled monolayer of germanium that forms a nearly flat honeycomb nanosheets [18]. Germanene shows strong spin–orbit coupling for topological insulator properties. Stanene, on the other hand, is derived from tin (α-Sn). Stanene is epitaxially grown on various substrates; however, its structure is not well-defined [18, 19].

From the group V elements, phosphorene or black phosphorus (BP) is an allotrope of phosphorous which is known to be thermodynamically stable at room temperature (RT). It also emerges as one of the novel 2D semiconducting materials which has similar properties and colour of graphite. Typically, BP has an orthorhombic crystal structure, closely analogous to graphene. In the crystal arrangement, the phosphorous atoms are organized in a honeycomb lattice with puckered double layers. BP monolayer has $sp^3$ hybridization where one phosphorous atom is covalently bonded to three other adjacent phosphorous atoms having a bond length of 2.18 Å [20]. In addition, it has one lone pair of electrons, thus forming a quadrangular pyramid structure. The adjacent layers of phosphorous atoms interact by weak vdW interactions where the distance between two layers is about 0.5 nm. Similarly, arsenene also belongs to group V that has a single buckled honeycomb 2D layer of arsenic. Arsenene has an indirect bandgap of 2.49 eV and a high charge carrier mobility. Another 2D structures are antimonene and bismuthene which are extracted buckled honeycomb network of antimony and bismuth [19]. Antimonene has high carrier mobility and excellent thermal conductivity. Bismuthene is extensively used in topological insulators through the reduction of bismuth [ref]. Notably, various structures and properties of BP-like puckered structures (α-phase) of arsenene, antimonene, and bismuthene have been predicted [18–20]. However, fabrication of monolayer α-phase is challenging mainly due of the lack of layered allotropes.

***MXenes***: With the expansion of the family of 2D nanomaterials, the derivatives of transition metals using carbides, carbonitrides, and nitrides lead to the discovery of MAX phases where M stands for transition metal (Ti, Zr, Cr, etc.), A is an element from A-group mainly IIIA, IVA (Ga, Pb, Al, etc.), and X is either carbon or nitrogen. By introducing selective etching of the A element from the MAX phases, MXenes are created. MXenes are considered as layered solids linked by strong metallic, ionic, and covalent bonds. Having a layered hexagonal structure, they belong to space group $P6_3/mmc$ symmetry. MXenes have a general formula $M_{n+1}AX_n$, with $n = 1$–3, and thereby, the MXene sheets consist of 3, 5, or 7 atomic layers constructing $M_2X$, $M_3X_2$, and $M_4X_3$, respectively [9]. Some examples of MXenes are $Ti_2C$, $Ti_3C_2$, $Mo_2Ga_2C$, $Nb_4C_3$, etc.

## 2 Synthesis of 2D Nanomaterials

The 2D nanomaterials possess both similarities and differences in their fundamental crystalline features compared to their 3D counterparts. Therefore, to maintain their unique structural/crystalline features and simultaneously retaining their outstanding properties, atomically thin 2D nanomaterials have become the forefront in condensed matter physics, materials science, and nanotechnology. In literature, there are numerous methods available for the synthesis of 2D nanomaterials. However, before addressing the individual experimental techniques, it is worth mentioning that the nanoscale synthesis methods are broadly categoried into two types: bottom-up approach and top-down approach (Fig. 2) [21].

### *2.1 Bottom-Up Approach*

The bottom-up approach is also referred as the gathering-up method in which the 2D nanomaterials can be synthesized from atomic or molecular precursors in the form of nanoparticles or nanocrystals that are allowed to grow in size after undergoing certain chemical reactions. The nanoscale particles thus self-assembled into larger complex substances or can be supplemented to any substrate of interest [21, 22]. The bottom-up approach is mainly desired for achieving controlled size, shape, composition, sequential stacking arrangement, and stable chemical structure. There are various synthetic methods used to prepare 2D nanomaterials using the bottom-up approach such as hydrothermal or solvo-thermal method, wet chemical synthesis, CVD, PECVD, organic ligand-assisted synthesis, interface-assisted synthesis, and template-assisted synthesis [23, 24]. Here, we have discussed the most regularly used techniques.

*Hydrothermal method*: This is one of the most common and widely used synthesis methods of 2D nanomaterials. It is cleared from the name itself that this technique deals with water (hydro) and heat (thermal). This means that this method is somewhat analogous to wet thermal synthesis. Although there are few additional requirements in the hydrothermal method which are the high temperature and pressure. Typically, the hydrothermal reaction is carried out inside an autoclave (vessel) with a Teflon liner. At first, the precursor materials are mixed thoroughly in an appropriate concentration and then transferred to the autoclave vessel. The autoclave vessel is designed in such a manner so that it can easily work under high-pressure conditions. Finally, the precursor-filled vessel is placed in a heating furnace, setting a specific temperature and time for the reaction to start till completion. Here, the solvents serve as the catalyst to initiate the reaction and help the growth of nanostructures [25]. This technique has several benefits such as high product yield, controlled size/shape, high-quality crystals, and most importantly, the low-cost instrumentation with environment-friendly synthesis. Yin et al. have presented a novel hydrothermal strategy to synthesize

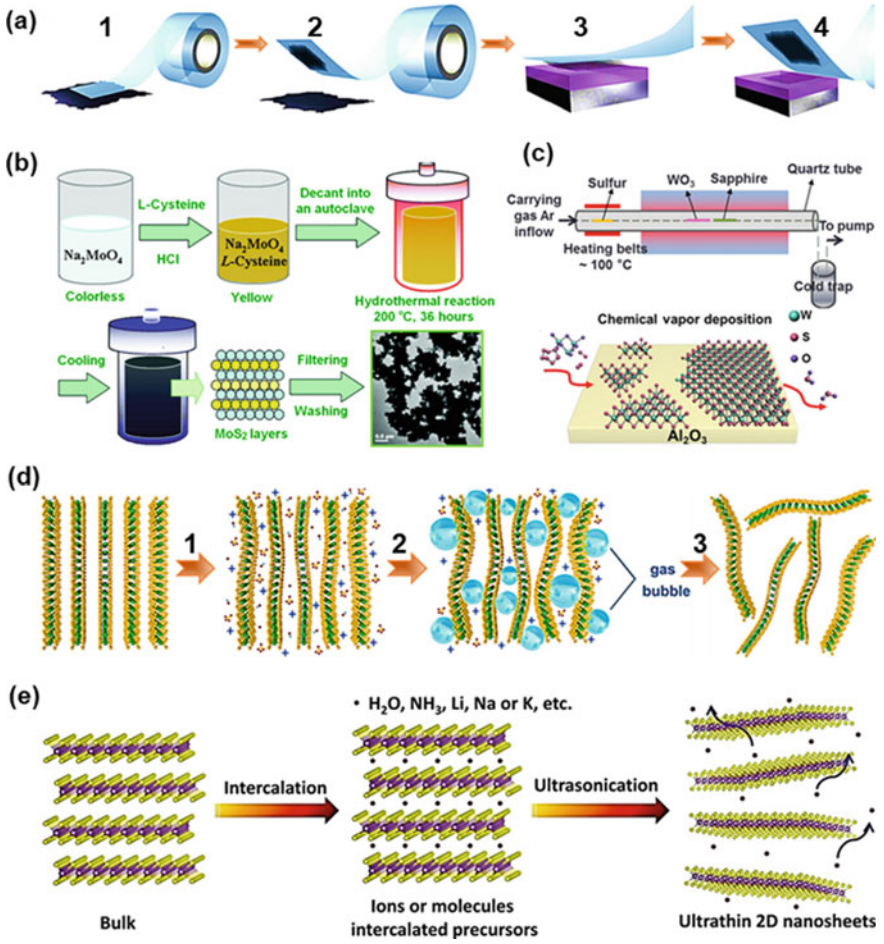


**Fig. 2** Different synthesis techniques for the growth of 2D nanomaterials: top-down and bottom-up approaches. **a** Mechanical cleavage method (1) press the adhesive tape against the 2D crystals, (2) few layers are attached to the tape, (3) the tape with crystals is pressed against a surface, (4) upon peeling, the bottom layer left on the substrate, **b** hydrothermal method, **c** CVD technique, **d** sonication derived exfoliation via (1) the addition of exfoliating/stabilizing agents, (2) sonication, and (3) exfoliated 2D nanosheets. **e** Ion-intercalation method. Reprinted with copyright permission from [5–8, 10]

$MoSe_2$ nanosheets [26]. This synthetic approach provides the synergistic regulation of both crystal phase (1T) and disorder engineering. In addition, one modified approach using the hydrothermal technique is reported by Dai et al., where graphene-like $MoSe_2$ nanosheets are synthesized under the synergy of graphene and polyvinylpyrrolidone [27]. Moreover, Alam et al. have synthesized metal oxide-based 2D nanomaterials using Bi-$TiO_2$ nanotube/graphene nanocomposites through simple hydrothermal synthesis [28]. Similarly, various 2D nanosheets of metal oxides such

as $Ga_2O_3$, $ZnGa_2O_4$, and $MnGa_2O_4$ are prepared by hydrothermal synthesis [29]. These nanosheets exhibit a triangular/hexagonal configuration with ultrathin thickness. In addition, Peng et al. demonstrated the use of a modified hydrothermal route using some basic etching agent to synthesize 2D MXene ($Ti_3C_2$) [30]. They have also extended their route to other MXene such as $Nb_2C$. Subsequently, to boost the material yield of MXenes, Han et al. have adopted a facile hydrothermal-assisted intercalation approach to form 2D $Ti_3C_2T_x$ and achieved 74% yield which was conventionally limited to 20% [31]. Hydrothermal synthesis is also used to prepare 2D nanosheets of boron nitride. Xie et al. reported the hydrothermal exfoliation method where the bulk h-BN undergoes expansion with the insertion of $Li^+$ and then exfoliated into ultrathin 2D nanosheets [32]. Catalyst-free g-$C_3N_4$ is also prepared by the low-cost hydrothermal approach [33].

*Chemical vapour deposition (CVD) method*: As the name suggests, CVD is a gas phase deposition method for the preparation of thin films over any desired substrate. Here, the precursors (volatile or viscous liquids) are injected into the vacuumed sealed reaction chamber in the form of vapours/gases and are allowed to go through some specific chemical reactions at a specific ambient temperature. Consequently, the placed substrates get coated when the reaction products of the precursors are assembled onto it [23, 34]. There are various synthesis parameters to take care of while performing the deposition such as process temperature, pressure, substrate temperature, and gas mixture composition. Therefore, simply controlling these parameters, it is possible to synthesize good quality thin films with high purity. This technique has some special advantages: for instance, low film porosity, high purity, and outstanding stability at air ambient comprehensively adopted in industries. Based on the CVD method, numerous 2D nanomaterials are synthesized for targeted applications. McCreary et al. reported the synthesis of large-area monolayers of $WS_2$ using CVD [35]. Likewise, Dankert et al. have worked on the fabrication of all CVD-based heterostructures with h-BN/graphene/h-BN configuration for developing high-performance Hall sensors [36]. As one kind of CVD technique, the researchers have also explored the PECVD technique to grow CN films using methane ($CH_4$) and $N_2$ gases [37]. Again, adopting an in-situ CVD approach, large-area 2D BP is grown with an average area of $> 3\ \mu m^2$ and about four layers of thickness [38]. A similar effort has been done by other groups to grow TMDs ($WS_2$) atomic layer on h-BN film by CVD technique [39].

*Interface-assisted synthesis*: Basically, an interface is referred as any flat or curved space (more precisely can be known as any phase boundary) between two dissimilar materials. Likewise, the interface formed between air and matter or between vacuum and matter is called the surface. Typically, the thickness of any interface ranges from angstrom (Å) to nanometres to few micrometres. Therefore, once the ratio of area to thickness in any interface is high enough, it is called a 2D interface. In the field of materials science, this 2D interface is highly active for multiple reactions as compared to the bulk phase. Some common interfaces that are involved in chemical reactions include the air/liquid, liquid/liquid, solid/liquid, and vacuum/solid interfaces. These types of 2D interfaces provide space to the precursors to gather and

induce the growth process or nucleation in a confined 2D space. This confined reaction in 2D space plays an important role in controlling the material properties of the final product [40]. Therefore, as one kind of bottom-up approach, there are various interface-assisted synthetic approaches reported in the literature for the development of 2D nanomaterials. Considering the synthesis of graphene (a star material in the field of materials science), the gas/solid or the vacuum/solid interface is a popular strategy that can be done using CVD. In CVD, a selective solid substrate is kept in a vacuumed/air chamber, and the gases of interest (say $CH_4$ for graphene) are inserted into the chamber which is allowed to react on the substrate. Pollard et al. confirmed the growth of graphene on a Ni film (Ni is used as a catalyst) deposited on the $SiO_2$/Si substrate using CVD [41]. Similarly, using CVD with a vapour/solid interface, h-BN is also synthesized by Shi et al. [42]. Interfacial synthesis strategies towards the preparation of TMDs have also been explored. Transition metal selenides such as $TiSe_2$, $NbSe_2$, and $TaSe_2$ are synthesized by surfactant lamellar templating which acts as efficient 2D catalysts. These 2D structures feature the thickness from single sheets to tens of nanometres [43]. Other noble 2D metal oxides such as $SnO_2$, CuO, and $In_2O_3$ are developed using surfactants. For the growth of 2D metal oxides using bottom-up approach from molecular precursors, Sun et al. have addressed the surfactant self-assembly, where the surfactants serve as the agents for structure design and help to confine the growth along the desired 2D direction [44]. In addition, an interesting 2D metal–oxide framework nanosheets are demonstrated by Nishihara and co-workers. At the air/water interface, they have tried to synthesize a single-layer nickel bis(dithiolene) nanosheets under atmospheric pressure [45]. Moreover, with regards to the other 2D nanomaterials such as MXenes, CN, and BP, the current synthesis methods are primly focused on the physical and chemical exfoliation of their bulk structures. Thus, the growth of single- to few-layered structures through the interface-assisted synthesis is still under progressive development.

## *2.2 Top-Down Method*

In contrast to the bottom-up approach, the top-down approach is more complex and requires sophistication. The top-down approach is also referred as the destructive method where the nanostructures are formed by removing the building blocks from the matter or cutting/sizing the solid crystal planes [21]. Particularly considering the synthesis of 2D nanomaterials, the top-down approach involves the breaking of interlayer spacing of a 3D matter to prepare atomically thin layers. Again, the top-down method is grouped into various types such as exfoliation method, chemical etching, sputtering, nano-lithography, and laser ablation. Here, we have discussed some of the widely used techniques:

*Exfoliation method*: The exfoliation method is categorized into two types: chemical exfoliation and physical exfoliation. Chemical exfoliation is resulted from the thinning of a layered crystal down to atomic-level layers through appropriate chemical

routes involving intercalants [46] to form 2D-layered structures. A large number of intercalants are used for chemical exfoliation such as acids/bases ($HSO_4^-$, $SO_2^{2-}$, and KOH), inorganic salts ($Li^+$, $Na^+$), oxidizing agents (hydrogen peroxide and hydroxyl radicals), and functional molecules ($NH^+$, pyrene sulfonic acid). Diazonium salts are effectively used to chemically exfoliate the semiconducting bulk $MoS_2$ in the 2H phase [47]. Similarly, some other bulk chalcogenides such as $Bi_2S_3$ and $Sb_2S_3$ are also exfoliated into 2D nanosheets using this chemistry [48, 49]. On the other hand, one report addresses that with aryldiazonium modification, it is possible to exfoliate bulk BP without undergoing any pre-treatment and passivation of the surface to form 2D nanosheets which can be applied in field-effect transistors (FET) [50]. Composites of graphene oxide/manganese phosphate are also realized by the chemical exfoliation process through Hummer's method as reported by Yuan et al. [51]. The liquid exfoliation method is also explored by many researchers for the synthesis of 2D metal oxides. This process is associated with gentle cutting of the bulk interlayers where different organic cations such as TBA and ammonium ions are used as the intercalant agents [52]. Chemical exfoliation of MAX phases into 2D MXenes is also highlighted by the research community. Khazaei et al. have utilized a series of first-principle calculations based on DFT and studied the exfoliation energies, forces, bond strengths, and electronic structures of the MAX phase. Based on their DFT calculations, around 37 MAX phases are proposed for successful exfoliation into 2D MXenes such as $Ti_3C_2$, $Ti_4C_3$, $Zr_2C$, $Hf_2C$, $V_3C_2$, $V_4C_3$, $Mo_2C$, and so on [53]. From the above-mentioned examples, now it is clear that with chemical exfoliation the chemical structure of 2D nanomaterials can be tuned through some appropriate reactions. During the chemical exfoliation process, sometimes the 2D nanomaterials suffer from loss of their inherent properties causing rapid degradation.

Physical exfoliation, on the other hand, can preserve the important properties of exfoliated 2D nanomaterials without experiencing much degradation. Physical exfoliation also offers large-scale production suitable for all practical applications. This type of exfoliation is mainly achieved through some external driving forces such as sonication, wet/dry ball milling, shear mixing, using some supercritical fluids, polar/non-polar solvents, and stabilizers. Considering the simplest case of ultrasonication, it has been reported by Kim et al. that any layered bulk material such as graphene, $MoS_2$, and h-BN can be exfoliated by controlling the temperature in an ultrasonic bath [54]. The as-exfoliated 2D materials, for instance, h-BN display an alternating charge distribution with a strong polarity across the boron and nitrogen termination edges. However, $MoS_2$ and $MoSe_2$ provide moderate polarity, where the surface has a negative charge with the sulphur atoms and counter-charges inside the molybdenum atoms. With ultrasonication, the 2D nanomaterials often suffer from the introduction of undesired defects. Therefore, the use of supercritical fluid is another approach to physical exfoliation [55]. As one of the most common supercritical fluids, $CO_2$ presents a solvent-like behaviour which can dissolve non-polar chemical species. Using $CO_2$, thick nanosheets of more than ten layers can be formed [56]. A molecular dynamics study is conducted for stabilizing MXene ($Ti_2CO_2$) structures using supercritical $CO_2$ as reported by Khaledialidusti et al. [57]. In addition, ball milling is also one type of physical exfoliation technique which is used to prepare

MXenes ($Ti_2C_2T_x$). After ball grinding, the $Ti_3AlC_2$ size is found to be uniform and can be tuned from 4.488 to 1.454 μm, with a well-defined 2D nanosheets structure [58]. Similarly, g-$C_3N_4$ powders are also synthesized by ball milling from amorphous carbon at high temperatures [59]. Graphene, TMDs, and h-BN synthesis with solvent-stabilizer exfoliation is also addressed using PVA-assisted shear-exfoliation and using chloroform/acetonitrile and IPA/water [60].

*Sputtering*: Sputtering is a comprehensively used industrial-based technique that provides large-scale high purity production of diverse materials maintaining high quality and controllability. With this technique, it is possible to use any kind of substrate and even applicable to insulating material deposition. In general, sputtering is performed under a vacuum with a target material to be sputtered. Generally, an inert gas (or a reactive gas) is used as a carrier gas to initiate the plasma glow upon applied bias. The ionized gases are then accelerated to the target material in the presence of an electric field and thus bombards the target surface with high kinetic energy, thereby ejection of the target atoms. Those target atoms are then self-assembled or accumulated on the substrates to form the smooth and uniform coating [61]. Various 2D nanomaterials are synthesized by sputtering. Rigi et al. have demonstrated a RF magnetron sputtering method to produce $MoS_2$ layers [62]. For the experiment molybdenum target was used under sulphur environment using an in-situ effusion cell. A highly pure 2H-$MoS_2$ phase is obtained using RF magnetron sputtering. Likewise, thin $MoSe_2$ interlayer is prepared by sputtering and selenization process by pressure variation and applied for efficient Cu(In, Ga)$Se_2$ solar cell (PCE = 10.8%) [63]. Moreover, high-quality boron nitride (BN) films are also deposited by magnetron sputtering as addressed by Sutter et al. [64]. Here, the boron is sputtered under $N_2$ and Ar environment, and the thickness of the deposited film is carefully controlled. Ensuring effective substrate temperature, two atomic layers of BN are successfully deposited by magnetron sputtering. Li et al. have reported an ionized magnetron sputtering method to deposit amorphous CN [65]. High purity graphite is used as the sputtering target with an inductively coupled plasma assembly between the target and the substrate under Ar/$N_2$ mixture gases. Within the $N_2$ to C ratio of 0.3–0.4, hardness up to 16–17 GPa is achieved. Moreover, Wang et al. using magnetron sputtering tried to deposit MXene with molybdenum carbide ($Mo_2C$) structure to be applicable in solid-state Q-switched pulsed laser generation [66]. The overall summary of the different synthetic approaches for the preparation of 2D nanomaterials including their advantages and challenges is tabulated in Table 1.

## 3 Properties and Characterizations of 2D Nanomaterials

The 2D nanomaterials based on their unique structures and wide range of synthetic approaches emerge as one of the novel classes of nanoscale materials. With the unique structural constructions of various 2D nanomaterials, they show interesting

**Table 1** Summary of various synthesis techniques to grow 2D nanomaterials with their achievements and challenges

| Synthetic methods | | 2D nanomaterials | Achievements | Challenges | References |
|---|---|---|---|---|---|
| Bottom-up | Hydrothermal/solvo-thermal method | TMDs: $MoSe_2$, $MoS_2$<br>Oxides: $Ga_2O_3$, $ZnGa_2O_4$, $MnGa_2O_4$<br>MXenes: $Ti_3C_2$, $Ti_3C_2T_x$<br>CN: g-$C_3N_4$ | • Easy processing<br>• High product yield<br>• Controlled size/shape<br>• Tunable morphology<br>• Low cost and eco-friendly | • Thickness control<br>• Long synthesis duration<br>• Repeatability<br>• Not scalable | [20–32] |
| | CVD, PECVD | TMDs: $WS_2$<br>h-BN<br>BP | • High purity<br>• Large-area coverage on any substrate<br>• Pin-hole free film<br>• Excellent stability<br>• High scalability | • Defect control<br>• High temperature<br>• High-cost sophisticated vacuum technique | [33–39] |
| | Interface-assisted synthesis | TMDs: $TiSe_2$, $NbSe_2$, $TaSe_2$<br>Oxides: $SnO_2$, CuO, and $In_2O_3$ | • Composition and design function<br>• Controlled size/shape<br>• Tunable morphology | • Small crystallites<br>• Thickness control<br>• Low-yield<br>• Inert atmosphere | [40–45] |
| Top-down | Exfoliation: Physical and chemical | TMDs: $MoS_2$, $Nb_2S_3$, $Sb_2S_3$<br>BP, silicene<br>MXenes: $Ti_3C_2$, $Ti_4C_3$, $Zr_2C$, $Hf_2C$, $V_3C_2$, $V_4C_3$, $Mo_2C$<br>CN: g-$C_3N_4$ | • High purity<br>• High porosity<br>• Uniform growth<br>• Wafer scalable | • Small crystallites<br>• Thickness control<br>• Low-yield<br>• Not scalable | [46–59] |
| | Sputtering | TMDs: $MoSe_2$, $MoS_2$<br>h-BN<br>MXenes: $Mo_2C$ | • High purity<br>• Large-area coverage on any substrate<br>• Pin-hole free film<br>• Excellent stability<br>• High scalability | • Defect control<br>• Comparatively high-cost technique | [60–66] |


**Fig. 3** Different properties of 2D nanomaterials with their corresponding unique characteristic features

properties like unprecedented optical or photonic properties and tunable morphological features. In addition, the 2D nanomaterials also offer unique electrical transport properties based on their dimensional restrictions. Moreover, the thermal, mechanical, and magnetic properties are also explored for some targeted applications with high stability (Fig. 3). Therefore, concerning the new synthesis approaches and vibrant properties, the 2D nanomaterials are realized in various applications related to material sciences such as in energy conversion (solar cells, water electrolysis, photocatalysis, thermoelectric devices, etc.) and energy storage devices (supercapacitors, batteries, etc.) [4–11]. In this section, we will elaborate on the individual properties shown by various 2D nanomaterials.

## *3.1 Structural Properties*

Geim and Novoselov won the Nobel Prize in 2004 for the invention of graphene which is an important class of 2D nanomaterial [2]. Graphene holds a hexagonal structure with $sp^2$ hybridized carbon atoms. The structure has alternate single and double bonds (i.e. a conjugated structure) with p-orbital overlapping and electron delocalization. Because of this structural arrangement, graphene holds a very stable crystalline form and offers unique properties such as high surface area, outstanding catalytic features, high optical transparency, and so on. Graphene has shown its potential as a promising candidate for diverse applications, for instance, in optoelectronics, supercapacitors, drug delivery, biosensors, and image sensors. Regardless of consuming numerous advantages and applications, graphene has some shortcomings too. For example,

the material is insoluble and infusible in nature. Therefore, for full utilization of graphene, some structural modifications are always required such as modifications in the basal plane, edges, and surface functionalization.

Now, expanding the portfolio of 2D nanomaterials from graphene, currently other new 2D materials such as TMDs, h-BN, g-$C_3N_4$, MXenes, and black phosphorous are in the forefront [4–10]. The sandwiched structured TMDs with X–M–X structure exhibit semiconducting properties with a tuneable bandgap which makes them a suitable candidate for optoelectronic devices [9]. Moreover, based on its unique layered structures, it is also used as an efficient catalyst material for applications in electrochemical cells [11]. $SnS_2$ belongs to the class of TMDs which crystallize in hexagonal $CdI_2$ lattice structure. It shows n-type semiconducting characteristics and is known to have a wide bandgap (2.03–2.4 eV) [67]. Its strong anisotropy makes it possible for its use in efficient holographic recording systems. Moreover, other TMDs such as $MoS_2$, $MoSe_2$, $WS_2$, and $TaS_2$ have out-of-plane mirror symmetry and in-plane inversion symmetry, owing to which they show complementary characteristics to that of graphene [9]. Also, in some cases, even these TMDs surpass the performance of graphene. The main uniqueness of these TMDs is their strong spin–orbit interaction. The most studied $MoS_2$ is a semiconductor with a 2H phase and tuneable bandgap from 1.2 to 1.9 eV. In addition, the $MoS_2$ monolayers have in-plane Young's modulus of 200–300 GPa. Another special parameter is its high mobility (> 190 $cm^2\ V^{-1}\ s^{-1}$), high on/off current ratio ($10^8$), and polarization properties. As such, $MoS_2$ shows potential applications in several fields such as nano-electronics, solar cells, chemosensing, energy storage, and catalysis [9, 68]. Tran et al. recently announced a new member of the MXene family: $V_4C_3T_x$ which is prepared by means of chemical exfoliation of the MAX phase ($V_4AlC_3$) using aqueous hydrofluoric acid [69]. The successfully exfoliated MXene $V_4C_3T_x$ is confirmed from the SEM morphology and STEM characterizations. In parallel, Rosen's group has addressed the synthesis of quaternary MAX solution with $(Nb_{2/3}Sc_{1/3})_2AlC$ structure. They have selectively etched both Al and Sc atoms to produce $Nb_{1.33}CT_x$ MXene, which is confirmed from XRD, XPS, and STEM [70]. Likewise, h-BN also belongs to the family of 2D nanomaterials which has a noteworthy structural resemblance to graphene. The 2D h-BN comprises both armchair and zigzag edge-terminated structures, where the layers are coupled to one another by the relatively weak vdW forces. The h-BN offers a high surface area and improved stability [12]. Silva et al. have demonstrated the synthesis of nanostructured BN through thermal CVD at 1150 °C. For this, iron compound ($FeS/Fe_2O_3$) is used as the catalyst on $Al_2O_3$ nanostructures [71].

## *3.2 Optical and Photonic Properties*

As already highlighted, the 2D nanomaterials provide diverse properties suitable for a broad spectrum of applications. One important property is the optical/photonic response of the 2D nanomaterials. The optical characteristics of materials are mostly

determined by the electronic band structure. The precise engineering of the electronic bands in 2D nanomaterials yields useful optical properties. It is well known that every 2D nanostructured material shows different optical bandgaps based on their individual structure–property relationship. The layered 2D halide perovskites show unprecedented optical properties with a tunable bandgap suitable for optoelectronic applications such as photodetectors, solar cells, and light-emitting diodes. [72]. $MA_3Bi_2I_9$, $Cs_2PbI_2Cl_2$, and $(BA)_2(MA)_2Pb_3I_{10}$ have a 2D-layered structure with bandgaps ranging from 1.5 to 1.9 eV. As one of the typical layered perovskite derivatives, these are used in solar cells and photodetectors [73]. Moreover, some 2D nanomaterials have large electronic bandgaps such as TMDs, h-BN, and MXenes. In particular, significant changes occur in the optical properties of TMDs due to the existence of indirect-to-direct bandgap transition. This depends on varying the thicknesses of $MoS_2$ layers. Monolayered $MoS_2$ with an energy bandgap of 1.8 eV can detect green light, whereas a triple-layered $MoS_2$ with a bandgap of 1.35 eV responds towards red light [74]. Moreover, h-BN and BP are also being investigated extensively for their photonic and optoelectronic properties. Brar et al. have demonstrated the surface phonon–plasmon–polariton modes in a heterostructure based on graphene and h-BN. They have shown experimentally that the plasmon mode of graphene is split into two modes which display anti-crossing behaviour near the energy of h-BN optical phonon at 1370 $cm^{-1}$ [75]. Preparation of g-$C_3N_4$ nanosheets incorporating plasmonic silver as an efficient photocatalyst is also explored for enhanced visible-light photocatalysis experiments. Deng et al. have studied the improved photocatalytic activity of plasmonic Ag and $N_2$ doped graphene QDs which are co-decorated on g-$C_3N_4$ nanosheets [76]. The experimental findings reveal an improved photocatalytic activity with 92.8% removal efficacy under white light and NIR irradiation. Plasmonic photodetection of MXenes is also reported based on its atomically thin layers. Velusamy et al. have reported $Mo_2CT_x$ MXene thin films which are successfully deposited on paper substrates. The as-fabricated photodetectors with this MXene structure exhibit extended photoresponse within 400–800 nm along with a high responsivity of 9 $AW^{-1}$ and detectivity of $5 \times 10^{11}$ Jones. It also exhibits reproducible photo-switching featured at a wavelength of 660 nm [77]. Moreover, a photodetector based on black phosphorous is also reported by Engel et al. for high-speed imaging [78]. Here, a multi-layered BP is capable of acquiring high contrast in the visible and infrared region of the electromagnetic spectrum showing its applicability for broadband optical detection.

## *3.3 Electrical Properties*

Electronic/electrical property is influenced by the presence of localized or delocalized transport of electrons in a solid material. Based on the electronic properties of various materials, the economy of numerous industries has improved by adopting state-of-the-art fabrication technologies. For the case of 2D nanomaterials, the electrons or holes are restricted to occupy the quantized energy levels in one spatial dimension.

Based on this, various important electronic properties are arising related to the energy level, transport, and phonon scattering and excitation in 2D nanomaterials.

Numerous heterostructures have been designed based on graphene for bandgap engineering such as graphene/h-BN, graphene/ZnO, and graphene/$MoS_2$ [79, 80]. In general, TMDs hold a vast range of electronic properties, from semi-metals to semiconductors to insulators. Xiong et al. reported the lithium intercalation in $MoS_2$ [81]. Because of Li insertion into the interlayer spacing, the electrical conductivity enhanced 200 times. Likewise, electrical transport in various TMDs has been investigated such as in 2H-$NbS_2$, -$NbSe_2$, -$TaS_2$, and $TaSe_2$, respectively. Here, to investigate the carrier scattering mechanisms, the charge density wave (CDW) system is used. Based on this, the measurements of the resistivity and the Hall coefficient of 2H-TMDs are carried out between 4.2 and 300 K [82]. The resistivity of 2H–$NbS_2$ displays no CDW transition. On contrary, 2H–$TaSe_2$ shows the highest CDW transition and along with several anomalous features. The electrical properties of MXene structure $Ti_3C_2T_x$ monolayers are investigated by Miranda et al. [83]. They have demonstrated the metallic nature of MXene with a high free carrier density of $8 \pm 3 \times 10^{21}$ $cm^{-3}$ and high mobility of $0.7 \pm 0.2$ $cm^2$ $V^{-1}$ $s^{-1}$. Based on the electrical performance of MXenes, they have been successfully utilized as promising candidates for energy storage applications, for example, in Na, Li, K ion batteries, supercapacitors, and fuel cells. As a 2D equivalent of graphene, the electrical properties of h-BN are also studied both individually and by forming heterostructure of graphene and h-BN [84]. In general, h-BN is considered as an insulator with a wide bandgap; however, forming the heterostructure with graphene (graphene/h-BN) for transistor application, the electron mobility and the drain current switching ratios are as high as 573 $cm^2$ $V^{-1}$ $s^{-1}$ and $-2 \times 10^{11}$ $cm^{-2}$ [85]. Moreover, the electrical properties of sputter-deposited CN thin films are also studied by Broitman et al. [86]. They have reported that by increasing the $N_2$ content during sputtering, the resistivity decreases from $4 \times 10^{-2}$ Ω-cm to $4 \times 10^{-3}$ Ω-cm. The electrical conductivity of BP has been measured by Keyes et al. [87]. They observed p-type conductivity under low temperatures. The electron and hole mobilities at room temperature are reported to be 350 and 220 $cm^2$ $V^{-1}$ $s^{-1}$, respectively.

### *3.4 Thermal Properties*

Thermal property management is an essential subject for designing robust electronic devices. 2D nanomaterials based on the thermoelectric effects can directly convert heat into electricity for harnessing waste heat. For this, mainly the Seebeck effect is used to modulate the conversion of heat into voltage [88]. Numerous studies were performed to achieve appreciable Seebeck coefficients. For instance, Hippalgaonkar et al. and Hewitt et al. have reported the Seebeck coefficients of $MoS_2$ and $Sb_2Te_3$ to be 8.5 mW-$m^{-1}$ $K^{-1}$ and 371 μW-$m^{-1}$ $K^{-1}$, respectively [89, 90]. In addition, among all the TMDs, $WS_2$ based on the Boltzmann transport equation provides the highest thermal conductivity of 142 $Wm^{-1}$ $K^{-1}$ followed by $MoS_2$ and $MoSe_2$ with

103 and 54 $Wm^{-1}$ $K^{-1}$ [91]. It has been addressed that the heterostructures of 2D nanomaterials provide an ideal platform to study interfacial heat transport. The interface thermal conductance of $MoS_2$ on Au substrate is as high as 221 MW-$m^{-2}$ $K^{-1}$ [92]. Moreover, polymeric carbon nitride (PCN) is investigated for thermoelectric performance using molecular dynamic simulations. It is found that PCN has a high figure-of-merit, ZT ($ZT = S^2\sigma T/\kappa$, where S is the Seebeck coefficient, σ is the electronic conductivity, T is the absolute temperature, and κ is the thermal conductivity) of 0.52 at 300 K which contributes to n-type thermoelectric group materials [93]. Heterojunction devices based on graphene/h-BN also offer a high thermoelectric power factor of 10.35 W-$m^{-2}$ $K^{-1}$ [94]. Introduction of MXene ($Ti_3C_2T_x$) into $(Bi, Sb)_2Te_3$ matrix also provides improved thermoelectric performance with ZT of 1.3 within 300–475 K towards high thermoelectric conversion efficiency [95].

## *3.5 Mechanical and Magnetic Properties*

Mechanical properties of 2D nanomaterials play an important role in various applications. Some mechanical properties include the fracture strengths, Young's modulus, elasticity, etc. [96]. One of the ways to control the mechanical properties of 2D nanomaterials is based on defect engineering, which helps to enhance the toughness of classical materials from metals to semiconductors to insulators [97].

Magnetic properties of 2D nanomaterials are of utmost importance which can find interest in applications related to electric motors, computers, and medical diagnosis. For example, ferromagnetism is considered as one of the intrinsic properties of atomically thin layered 2D materials at room temperature [98]. This property has also shown a broader prospect for nano-device design. In particular, for spintronic applications, the intrinsic magnetic orders in ultrathin 2D nanomaterials have been extensively studied [99]. Sanikop et al. have tried to tailor the magnetically active sites of $MoS_2$ nanosheets for spintronic applications [100]. For this, defect-density controlled 2H phase of $MoS_2$ nanosheets is prepared at 500–900 °C which shows a ferromagnetic-like transition at 120 K. Likewise, Du et al. have elaborated the first-principle prediction of metal-free magnetism in g-$C_3N_4$ [101]. The ferromagnetic ground state displayed by the g-$C_4N_3$ also possesses an intrinsic half-metallicity. Kumar et al. have demonstrated the intrinsic ferromagnetism in $Mn_2NT_x$, $Ti_2NO_x$, and $Cr_2NO_x$, MXene structures [102]. High magnetic moments, high Curie temperature (1877 K), and robust ferromagnetism are found in these MXenes for spintronic applications. Furthermore, in the heterostructure of $Ni(OH)_2$ and h-BN, a larger magnetic moment with ferromagnetic coupling is found [40]. Furthermore, ferromagnetic 2D nanomaterials with superior electronic and optical properties are used for the construction of compact magnetic, magneto-electronic, and magneto-optical devices. Table 2 provides an overview of all the unique properties of various 2D nanomaterials.

**Table 2** Summary of different properties of various 2D nanomaterials

| 2D material | Properties | | | | | | | References |
|---|---|---|---|---|---|---|---|---|
| | Structural | Optical | Electrical | Thermal | Mechanical | | Magnetic | |
| | Phase; Thickness (Å) | $E_g$ (eV) | Mobility ($cm^2 V^{-1} s^{-1}$) | Thermal conductivity ($Wm^{-1} K^{-1}$) | Young's modulus (GPa) | Fracture strength (GPa) | | |
| g-$C_3N_4$ | Hexagonal, rhombic; 3.35 | 0.98–3.34 | $3 \times 10^5$ | 7.6 | 822 | 45.4(Z), 31.4(A) | Ferromagnetic metal | [59, 76, 86, 93] |
| $MoS_2$ | 2H, 1T, 3R, 1T'; 6.04 | 1.2–1.9 (2H) | > 190 | 103 | 219(Z), 222(A) | 16.9(Z), 7.3(A) | RT ferromagnetic | [8, 89, 92, 99] |
| $WS_2$ | 2H, 1T; 0.608 | 1–2 (2H) | 140 | 142 | 240(Z), 244(A) | 19.9(Z), 29.9(A) | Ferromagnetic, anti-ferromagnetic, and metallic | [35, 39, 91] |
| $MoSe_2$ | 2H, 1T; 0.637 | 1.1–1.55 | 121 | 54 | 175(Z), 178(A) | – | Anti-ferromagnetic | [26, 27, 63] |
| $MoTe_2$ | 2H, 1T'; 0.691 | < 1 (2H), 60 m (1T') | 4000 | 0.35 | 205 | – | Diamagnetic and paramagnetic | [8, 96] |
| $WSe_2$ | 2H, 1T; 0.641 | 1.4–1.6 | 66 | 3.935 | 194(Z), 196(A) | 15.0(Z), 24.7(A) | Ferromagnetic upon doping and creating defects in $WSe_2$ | [8, 96] |

(continued)

**Table 2** (continued)

| 2D material | Properties | | | | | | | References |
|---|---|---|---|---|---|---|---|---|
| | Structural | Optical | Electrical | Thermal | Mechanical | | Magnetic | |
| | Phase; Thickness (Å) | $E_g$ (eV) | Mobility ($cm^2 V^{-1} s^{-1}$) | Thermal conductivity ($Wm^{-1} K^{-1}$) | Young's modulus (GPa) | Fracture strength (GPa) | | |
| $WTe_2$ | 1T'; 0.691 | 55 m | 74 | 3 | 135(Z), 137(A) | 9.30(Z), 18.7(A) | RT ferromagnetic upon doping | [8, 96] |
| h-BN | Hexagonal; 3.34 | 5–6 | 573 | 10.35 | 865 | 70.5 | RT ferromagnetic upon doping | [40, 85, 94, 96] |
| BP | Cubic, rhombohedral; 5.55 | 0.3–2.3 | 350–220 | 40 | 166(Z), 44(A) | 18(Z), 8(A) | Non-magnetic, but shows ferromagnetic upon doping and creating defects in BP | [87, 96] |
| Silicene | $(\sqrt{3} \times \sqrt{3})R30^o$; 4.20 | 1.55 m | $2.5 \times 10^5$ | 5.4 | 82.2 | 12.5 | Ferromagnetic upon doping and creating defects silicene | [18, 19, 96] |
| Bismuthene | Hexagonal; 4.94 | 0.5 | $5.7 \times 10^6$ | 1.3 | 26.1 | 25.5 | Ferromagnetic upon doping | [18, 19, 96] |
| $Ti_3C_2$ | Hexagonal; 3 | 3 | 2.6 | 11.57 | 80–100 | – | RT Ferromagnetic | [9, 30] |

***$E_g$*** bandgap, *A* armchair, *Z* zigzag, *RT* room temperature

## 4 Future Aspects and Conclusions

This chapter offers an overview of the fundamentals of 2D nanomaterials including their structure, types, synthesis, and properties. It is now well established that 2D nanomaterials are the special class of materials which open up a new avenue of diverse applications including energy conversion, storage, and in the environment and biomedical fields. We have mainly highlighted the 2D nanomaterials based on TMDs ($MoS_2$, $WSe_2$, $MoSe_2$, etc.), BP, g-$C_3N_4$, h-BN, MXenes, 2D metal oxides, and layered perovskites. The 2D nanomaterials can be synthesized from various routes, among which we have discussed in detail the bottom-up and top-down approaches. Finally, numerous interesting properties including structural, optical, electrical, mechanical, thermal, and magnetic properties are elaborated with examples of 2D nanomaterials. Based on the special properties of 2D nanomaterials, significant applications are highlighted related to energy conversion technologies suitable for energy harvesting and energy storage devices. However, the commercialization of 2D nanomaterials is still in the progressing stage of technology.

With the intervening time, nanotechnology has been revolutionized by the use of 2D nanomaterials. 2D nanomaterials cover a number of important topics in basic and applied sciences making a novel class of materials with a promising future. 2D nanomaterials with high surface area, high electronic and excellent optical properties will be very useful in the near future for nano-electronic applications to be utilized in lithium-ion batteries, image sensors, biosensors, solar cells, supercapacitors, and catalysts. However, it is noteworthy that the cost of 2D nanomaterials is relatively higher, but as technologies will reach the maturing phase, the use of 2D nanomaterials will nurture, thus enabling the higher demand for targeted applications with lower prices that may start to establish themselves in the marketplace. It is anticipated that the contents summarized in this chapter can afford an important reference and guideline for further systematic studies on 2D nanomaterials.

**Acknowledgements** This study is financially supported by the Department of Science and Technology (DST), Government of India, under the Inspire Faculty Award (DST/INSPIRE/04/2018/001721).

## References

1. Jitendra NT, Rajanish NT, Kwang SK (2012) Zero-dimensional, one-dimensional, two-dimensional, and three-dimensional nanostructured materials for advanced electrochemical energy devices. Prog Mater Sci 57:724–803
2. Novoselov KS, Geim AK, Morozov SV et al (2004) Electric field effect in atomically thin carbon films. Science 306:666–669
3. Huang X, Zeng ZY, Zhang H (2013) Metal dichalcogenide nanosheets: Preparation, properties and applications. Chem Soc Rev 42:1934–1946
4. Cai Z, Liu B, Zou X et al (2018) Chemical vapor deposition growth and applications of two-dimensional materials and their heterostructures. Chem Rev 118:6091–6133

5. Han Y, Ge Y, Chao Y et al (2018) Recent progress in 2D materials for flexible supercapacitors. J Energy Chem 27:57–72
6. Novoselov KS, Neto AHC (2012) Two-dimensional crystals-based heterostructures: materials with tailored properties. Phys Scr T146:014006
7. Liu N, Kim P, Kim JH et al (2014) Large-area atomically thin $MoS_2$ nanosheets prepared using electrochemical exfoliation. ACS Nano 8:6902–6910
8. Zhang Y, Zhang Y, Ji Q et al (2013) Controlled growth of high-quality monolayer WS2 layers on sapphire and imaging its grain boundary. ACS Nano 7:8963–8971
9. Naguib M, Mochalin VN, Barsoum MW et al (2014) 25th anniversary article: MXenes: a new family of two-dimensional materials. Adv Mater 26:992–1005
10. Guo X, Wang Y, Wu F et al (2015) A colorimetric method of analysis for trace amounts of hydrogen peroxide with the use of the nano-properties of molybdenum disulfide. Analyst 140:1119–1126
11. Lin Y, Williams TV, Connell JW (2010) Soluble, exfoliated hexagonal boron nitride nanosheets. J Phys Chem Lett 1:277–283
12. Zhi C, Bando Y, Tang C et al (2009) Large-scale fabrication of boron nitride nanosheets and their utilization in polymeric composites with improved thermal and mechanical properties. Adv Mater 21:2889–2893
13. Zhao Z, Sun Y, Dong F (2015) Graphitic carbon nitride based nanocomposites: a review. Nanoscale 7:15–37
14. Osada M, Sasaki T (2009) Exfoliated oxide nanosheets: new solution to nanoelectronics. J Mater Chem 19:2503–2511
15. El-Ballouli A, Bakr OM, Mohammed OF (2020) Structurally tunable two-dimensional layered perovskites: from confinement and enhanced charge transport to prolonged hot carrier cooling dynamics. J Phys Chem Lett 11:5705–5718
16. Rodenas T, Luz I, Prieto G et al (2015) Metal-organic framework nanosheets in polymer composite materials for gas separation. Nat Mater 14:48–55
17. Peng Y, Li Y, Ban Y et al (2014) Metal-organic framework nanosheets as building blocks for molecular sieving membranes. Science 346:1356–1359
18. Bhimanapati GR, Zhong L, Vincent M et al (2015) Recent advances in two-dimensional materials beyond graphene. ACS Nano 9:11509–11539
19. Xiangkai K, Qiangchun L, Changlin Z et al (2017) Elemental two-dimensional nanosheets beyond graphene. Chem Soc Rev 46:2127–2157
20. Liu H, Du Y, Deng Y et al (2015) Semiconducting black phosphorus: synthesis, transport properties and electronic applications. Chem Soc Rev 44:2732–2743
21. Iqbal P, Preece JA, Mendes PM (2012) Nanotechnology: the "top-down" and "bottom-up" approaches. Supramol Chem Mol Nanomater. https://doi.org/10.1002/9780470661345.smc195
22. Xiao X, Wang H, Urbankowski P et al (2018) Topochemical synthesis of 2D materials. Chem Soc Rev 47:8744–8765
23. Jiang J, Li N, Zou J et al (2019) Synergistic additive-mediated CVD growth and chemical modification of 2D materials. Chem Soc Rev 48:4639–4654
24. Han ZJ, Murdock AT, Seo DH et al (2018) Recent progress in plasma-assisted synthesis and modification of 2D materials. 2D Mater 5:032002
25. Feng S, Xu R (2001) New materials in hydrothermal synthesis. Acc Chem Res 34:239–247
26. Yin Y, Zhang Y, Gao T (2017) Synergistic phase and disorder engineering in 1T-nanosheets for enhanced hydrogen-evolution reaction. Adv Mater 29:1700311
27. Dai C, Zhou Z, Tian C et al (2017) Large-scale synthesis of graphene-like $MoSe_2$ nanosheets for efficient hydrogen evolution reaction. J Phys Chem C 121:1974–1981
28. Alam U, Fleisch M, Kretschmer I et al (2017) One-step hydrothermal synthesis of Bi-$TiO_2$ nanotube/graphene composites: an efficient photocatalyst for spectacular degradation of organic pollutants under visible light irradiation. Appl Catal B 218:758–769
29. Yang W, Li J, Zhang X et al (2019) Hydrothermal approach to spinel-type 2D metal oxide nanosheets. Inorg Chem 58:549–556

30. Peng C, Wei P, Chen X et al (2018) A hydrothermal etching route to synthesis of 2D MXene ($Ti_3C_2$, $Nb_2C$): enhanced exfoliation and improved adsorption performance. Ceram Int 44:18886–18893
31. Han F, Luo S, Xie L et al (2019) Boosting the yield of MXene 2D Sheets via a facile hydrothermal-assisted intercalation. ACS Appl Mater Interfaces 11:8443–8452
32. Xie B, Li C, Chen J et al (2020) Exfoliated 2D hexagonal boron nitride nanosheet stabilized stearic acid as composite phase change materials for thermal energy storage. Sol Energy 204:624–634
33. Zhang P, Li X, Shao C et al (2015) Hydrothermal synthesis of carbon-rich graphitic carbon nitride nanosheets for photoredox catalysis. J Mater Chem A 3:3281–3284
34. Zhang Y, Zhang L, Zhou C (2013) Review of chemical vapor deposition of graphene and related applications. Acc Chem Res 46:2329–2339
35. McCreary KM, Hanbicki AT, Jernigan GG et al (2016) Synthesis of large-area $WS_2$ monolayers with exceptional photoluminescence. Sci Rep 6:19159
36. Dankert A, Karpiak B, Saroj P (2017) Dash hall sensors batch-fabricated on all-CVD h-BN/graphene/h-BN heterostructures. Sci Rep 7:15231
37. Khanis NH, Ritikos R, Azlinda S et al (2017) Investigations on the Role of $N_2$:($N_2$ + $CH_4$) ratio on the growth of hydrophobic nanostructured hydrogenated carbon nitride thin films by plasma enhanced chemical vapor deposition at low temperature. Mater 10:102
38. Smith JB, Hagaman D, Ji H-F (2016) Growth of 2D black phosphorus film from chemical vapor deposition. Nanotechnology 27:215602.
39. Okada M, Sawazaki T, Watanabe K et al (2014) Direct chemical vapor deposition growth of $WS_2$ atomic layers on hexagonal boron nitride. ACS Nano 8:8273–8277
40. Dong R, Zhang T, Feng X et al (2018) Interface-assisted synthesis of 2D materials: trend and challenges. Chem Rev 118:6189–6235
41. Pollard AJ, Nair RR, Sabki SN et al (2009) Formation of monolayer graphene by annealing sacrificial nickel thin films. J Phys Chem C 113:16565–16567
42. Shi Y, Hamsen C, Jia X et al (2010) Synthesis of new-layer hexagonal boron nitride thin film by chemical vapor deposition. Nano Lett 10:4134–4139
43. Brent JR, Savjani N, O'Brien P (2017) Synthetic approaches to two-dimensional transition metal dichalcogenide nanosheets. Prog Mater Sci 89:411–478
44. Sun Z, Liao T, Dou Y et al (2014) Generalized self-assembly of scalable two-dimensional transition metal oxide nanosheets. Nat Commun 5:3813
45. Kusamoto T, Nishihar H (2019) Zero-, one- and two-dimensional bis(dithiolato)metal complexes with unique physical and chemical properties. Coord Chem Rev 380:419–439
46. Le T-H, Oh Y, Kim H et al (2020) Exfoliation of 2D materials for energy and environmental applications. Chem Eur J 26:6360–6401
47. Lee H, Bak S, An S-J et al (2017) Highly efficient thin-film transistor via cross linking of 1T edge functional 2H molybdenum disulfides. ACS Nano 11:12832–12839
48. Dhar N, Syed N, Mohiuddin M et al (2018) Exfoliation behavior of van der waals strings: Case study of $Bi_2S_3$. ACS Appl Mater Interfaces 10:42603–42611
49. Li DO, Gilliam MS, Chu XS (2019) Covalent chemical functionalization of semiconducting layered chalcogenide nanosheets. Mol Syst Des Eng 4:962
50. Ryder CR, Wood JD, Wells SA (2016) Covalent functionalization and passivation of exfoliated black phosphorus via aryl diazonium chemistry. Nat Chem 8:597–602
51. Yuan R, Yuan J, Wu Y (2018) Graphene oxide-monohydrated manganese phosphate composites: preparation via modified Hummers method. Colloids Surf A 547:56–63
52. Zhang Q, Mei L, Cao X (2020) Intercalation and exfoliation chemistries of transition metal dichalcogenides. J Mater Chem A 8:15417–15444
53. Khazaei M, Ranjbar A, Esfarjani K (2018) Insights into exfoliation possibility of MAX phases to MXenes. Phys Chem Chem Phys 20:8579–8592
54. Kim J, Kwon S, Cho D-H (2015) Direct exfoliation and dispersion of two-dimensional materials in pure water via temperature control. Nat Commun 6:8294

55. Sun Z, Fan Q, Zhang M (2019) Supercritical fluid-facilitated exfoliation and processing of 2D materials. Adv Sci 6:1901084
56. Sasikala SP, Poulin P, Aymonier C (2016) Prospects of supercritical fluids in realizing graphene-based functional materials. Adv Mater 28:2663
57. Khaledialidusti R, Mahdaviab E, Barnoush A (2019) Stabilization of 2D graphene, functionalized graphene, and $Ti_2CO_2$ (MXene) in super-critical $CO_2$: a molecular dynamics study. Phys Chem Chem Phys 21:12968–12976
58. Huang S, Mochalin VN (2019) Hydrolysis of 2D transition-metal carbides (MXenes) in colloidal solutions. Inorg Chem 58:1958–1966
59. Zhen F, Yu-Xian L (2003) Carbon nitride compounds synthesized by thermal annealing amorphous nanostructured graphite under the flow of $NH_3$ gas. Chin Phys Lett 20:1540–1543
60. Khanam Z, Liu J, Song S (2020) Flexible graphene paper electrode prepared via polyvinyl alcohol-assisted shear-exfoliation for all-solid-state polymer supercapacitor application. Electrochim Acta 363:137208
61. Kelly PJ, Arnell RD (2000) Magnetron sputtering: a review of recent developments and applications. Vacuum 56:159–172
62. Rigi VJC, Jayaraj MK, Saji KJ (2020) Envisaging radio frequency magnetron sputtering as an efficient method for large scale deposition of homogeneous two-dimensional $MoS_2$. Appl Surf Sci 529:147158
63. Lin W-T, Chan S-H, Tseng S-Z (2014) Manipulation of $MoSe_2$ films on CuIn(Ga)Se2 solar cells during rapid thermal process, Int J Photoenergy 253285
64. Sutter P, Lahiri J, Zahl P (2013) Scalable synthesis of uniform few-layer hexagonal boron nitride dielectric films. Nano Lett 13:276–281
65. Li D, Lopez S, Chung YW et al (1995) Ionized magnetron sputter deposition of amorphous carbon nitride thin films. J Vac Sci Technol A 13:1063
66. Wang J, Liu S, Wang Y et al (2020) Magnetron-sputtering deposited molybdenum carbide MXene thin films as a saturable absorber for passively Q-switched lasers. J Mater Chem C 8:1608–1613
67. Ye G, Gong Y, Lei S et al (2017) Synthesis of large-scale atomic-layer $SnS_2$ through chemical vapor deposition. Nano Res 10:2386–2394
68. Bazaka K, Levchenko I, Wei J et al (2019) $MoS_2$–based nanostructures: synthesis and applications in medicine. J Phys D: Appl Phys 52:183001
69. Tran MH, Schafer T, Shahraei A et al (2018) Adding a new member to the MXene family: synthesis, structure, and electrocatalytic activity for the hydrogen evolution reaction of $V_4C_3T_x$. ACS Appl Energy Mater 1:3908–3914
70. Lu J, Thore A, Meshkian R et al (2017) Theoretical and experimental exploration of a novel in-plane chemically ordered $(Cr_{2/3}M_{1/3})_2AlC$ i-MAX Phase with M = Sc and Y. Cryst Growth Des 17:5704–5711
71. Silva WH, Ribeiro H, Ferreira TH et al (2017) Synthesis of boron nitride nanostructures from catalyst of iron compounds via thermal chemical vapour deposition technique. Phys E 89:177–182
72. Mao L, Stoumpos CC, Kanatzidis MG (2019) Two-dimensional hybrid halide perovskites: principles and promises. J Am Chem Soc 141:1171–1190
73. Blancon J-C, Even J, Stoumpos CC et al (2020) Semiconductor physics of organic–inorganic 2D halide perovskites. Nat Nanotechnol 15:969–985
74. Lopez-Sanchez O, Lembke D, Kayci M et al (2013) Ultrasensitive photodetectors based on monolayer $MoS_2$. Nat Nanotechnol 8:497–501
75. Brar VW, Jang MS, Sherrott M et al (2014) Hybrid surface-phonon-plasmon polariton modes in graphene/monolayer h-BN heterostructures. Nano Lett 14:3876–3880
76. Deng Y, Tang L, Feng C et al (2017) Construction of plasmonic Ag and nitrogen-doped graphene quantum dots codecorated ultrathin graphitic carbon nitride nanosheet composites with enhanced photocatalytic activity: full spectrum response ability and mechanism insight. ACS Appl Mater Interfaces 9:42816–42828

77. Velusamy DB, El-Demellawi JK, El-Zohry AM et al (2019) MXenes for plasmonic photodetection. Adv Mater 31:1807658
78. Engel M, Steiner M, Avouris P (2014) Black phosphorus photodetector for multispectral, high-resolution imaging. Nano Lett 14:6414–6417
79. Sutter P, Cortes R, Lahiri J et al (2012) Interface formation in monolayer graphene-boron nitride heterostructures. Nano Lett 12:4869–4874
80. Wang S, Tian H, Ren C et al (2018) Electronic and optical properties of heterostructures based on transition metal dichalcogenides and graphene-like zinc oxide. Sci Rep 8:12009
81. Xiong F, Wang H, Liu X et al (2015) Li intercalation in $MoS_2$: in situ observation of its dynamics and tuning optical and electrical properties. Nano Lett 15:6777–6784
82. Liu Y, Shao DF, Li LJ et al (2016) Nature of charge density waves and superconductivity in $1T-TaSe_{2-x}Te_x$. Phys Rev B 94:045131
83. Miranda A, Halim J, Lorke A et al (2017) Rendering $Ti_3C_2T_x$ (MXene) monolayers visible. Mater Res Lett 5:322–328
84. Wang J, Ma F, Liang W et al (2017) Electrical properties and applications of graphene, hexagonal boron nitride (h-BN) and graphene/h-BN heterostructures. Mater Today Phys 2:6–34
85. Wang X, Hossain M, Wei Z et al (2019) Growth of two-dimensional materials on hexagonal boron nitride (h-BN). Nanotechnology 30:034003
86. Broitman E, Hellgren N, Neidhardt J et al (2002) Electrical properties of carbon nitride thin films: role of morphology and hydrogen content. J Electron Mater 31:L11–L15
87. Keyes RW (1953) The electrical properties of black phosphorus. Phys Rev 92:580
88. Li D, Gong Y, Chen Y et al (2020) Recent progress of two-dimensional thermoelectric materials. Nano-Micro Lett 12:36
89. Hippalgaonkar K, Wang Y, Ye Y et al (2017) High thermoelectric power factor in two-dimensional crystals of $MoS_2$. Phys Rev B 95:115407
90. Hewitt CA, Li Q, Xu J et al (2017) Ultrafast digital printing toward 4D shape changing materials. Adv Mater 29:1605390
91. Gu X, Yang R (2014) Phonon transport in single-layer transition metal dichalcogenides: a first-principles study. Appl Phys Lett 105:131903
92. Ding Z, Pei Q-X, Jiang J-W et al (2016) Interfacial thermal conductance in graphene/$MoS_2$ heterostructure. Carbon 96:888–896
93. Ding Z, An M, Mo S et al (2014) Unexpectedly high cross-plane thermoelectric performance of layered carbon nitrides. J Mater Chem A 7:2114
94. Duan J, Wang X, Lai X et al (2016) High thermoelectric power factor in graphene/hBN devices. PNAS 113:14272–14276
95. Lu X, Zhang Q, Liao J (2020) High-efficiency thermoelectric power generation enabled by homogeneous incorporation of MXene in (Bi, $Sb_)2T_e3$ Matrix. Adv Energy Mater 10:1902986
96. Liu B, Zhou K (2019) Recent progress on graphene-analogous 2D nanomaterials: properties, modeling and applications. Prog Mater Sci 100:99e169
97. Deji A, Christopher JB, Scott BJ et al (2017) A review on mechanics and mechanical properties of 2D material-graphene and beyond. Extreme Mech Lett 13:42–77
98. Miao N, Xu B, Zhu L et al (2018) 2D Intrinsic ferromagnets from van der Waals antiferromagnets. J Am Chem Soc 140:2417–2420
99. Miller JL (2017) Ferromagnetism found in two-dimensional materials. Phys Today 70:16
100. Sanikop R, Sudakar C (2020) Tailoring magnetically active defect sites in $MoS_2$ nanosheets for spintronics applications. ACS Appl Nano Mater 3:576–587
101. Du A, Sanvito S, Smith SC (2012) First-principles prediction of metal-free magnetism and intrinsic half-metallicity in graphitic carbon nitride. Phys Rev Lett 108:197207
102. Kumar H, Frey NC, Dong L et al (2017) Tunable magnetism and transport properties in nitride MXenes. ACS Nano 11:7648–7655